

Incorporating Cs and Sr into blast furnace slag inorganic polymers and their effect on matrix properties

Peer-reviewed author version

VANDEVENNE, Niels; Ion Iacobescu, Remus; Pontikes, Yiannis; CARLEER, Robert; THIJSSSEN, Elsy; GIJBELS, Katrijn; SCHREURS, Sonja & SCHROEYERS, Wouter (2018) Incorporating Cs and Sr into blast furnace slag inorganic polymers and their effect on matrix properties. In: JOURNAL OF NUCLEAR MATERIALS, 503, p. 1-12.

DOI: 10.1016/j.jnucmat.2018.02.023

Handle: <http://hdl.handle.net/1942/25994>

1 **Incorporating Cs and Sr into blast furnace slag inorganic polymers**
2 **and their effect on matrix properties**

3 Niels Vandevenne ^a, Remus Ion Iacobescu ^b, Yiannis Pontikes ^b, Robert Carleer ^c, Elsy Thijssen ^c, Katrijn Gijbels ^a,
4 Sonja Schreurs ^a, Wouter Schroeyers ^{a,*}

5 ^a *Hasselt University, CMK, Nuclear Technological Centre (NuTeC), Faculty of Engineering Technology, Agoralaan,*
6 *Gebouw H, 3590 Diepenbeek, Belgium*

7 ^b *KU Leuven, Department of Materials Engineering, Kasteelpark Arenberg 44, 3001 Leuven, Belgium*

8 ^c *Hasselt University, CMK, Research Group of Applied and Analytical Chemistry, Agoralaan, Gebouw D, 3590*
9 *Diepenbeek, Belgium*

10

11

12

13

* Corresponding author: Prof. dr. Wouter Schroeyers, e-mail address:

14

wouter.schroeyers@uhasselt.be

15

16 **Abstract**

17 Minimizing harmful effects to the environment in waste-management practices requires continuous
18 innovation. This is especially important in the field of radioactive waste management. Alternatives to
19 the commonly used ordinary Portland cement matrices are being increasingly studied for improved
20 immobilisation purposes. The development of inorganic polymers (IP) from industrial residues has
21 been successfully studied for the immobilisation of caesium (Cs^+) and strontium (Sr^{2+}). However,
22 knowledge of the effect of these introduced elements on the IP-matrix is scarce, especially
23 considering that studied effects are dependent on the IP-precursor characteristics and the form in
24 which the Cs^+ and Sr^{2+} are introduced. In this study, IPs containing varying amounts of CsNO_3 and
25 $\text{Sr}(\text{NO}_3)_2$ were developed to study the effect of the introduced elements on the IP-characteristics. IP-
26 samples were developed from ground granulated blast furnace slag (GGBFS) and 6 M NaOH
27 activating solution. Cs^+ and Sr^{2+} were added to account for 0.5, 1 and 2 wt% of the total IP-mass.
28 Throughout the entire study, Cs^+ -addition showed no significant effects on the studied parameters.
29 Calorimetric results showed that Sr^{2+} severely affects reaction kinetics, consuming hydroxide ions
30 necessary for the alkali activation reaction. Sr^{2+} -addition also caused a severe decrease in
31 compressive strength, increased calcium leaching, and decreased sodium and hydroxide leaching.
32 Micro-chemical analyses showed that Cs^+ is almost fully incorporated in the formed IP-matrix, while
33 Sr^{2+} mainly precipitates as $\text{Sr}(\text{OH})_2$ in concentrated regions throughout the IP-structure. The findings
34 presented in this paper give insights on the effect of contaminant elements on the immobilizing
35 matrix.

36 **Keywords**

37 **Inorganic polymer, waste immobilisation, slag, caesium, strontium, alkali activation**

38 1 Introduction

39 To address health and environmental risks associated with long-term storage of radioactive waste
40 (RAW), researchers have been looking for better performing alternatives to the ordinary Portland
41 cement (OPC) matrices vastly used by the nuclear industry for RAW-immobilisation; these
42 alternatives include calcium-sulfoaluminate-cement, calcium-aluminate-cement, and
43 geopolymer/inorganic polymer-type matrices (based on metakaolin and sodium silicate) [1].
44 Immobilising hazardous cations like caesium-137 ($^{137}\text{Cs}^+$, $T_{1/2} = 30.05$ a) and strontium-90 ($^{90}\text{Sr}^{2+}$, $T_{1/2} =$
45 28.80 a) is key in handling RAW, especially concerning nuclear power plants [2,3], since these
46 radionuclides are most often present in cooling water of nuclear reactors [4]. The main solidification
47 mechanism for cationic species in OPC-based binders, which is based on precipitation of the
48 corresponding hydroxides due to the highly alkaline pore solution, is not valid for Cs^+ causing a low
49 retention and high diffusion towards the biosphere [5]. According to Wieland et al. (2008), Sr^{2+} -
50 uptake in OPC occurs mainly as partially hydrated species, binding Sr^{2+} to calcium-silicate-hydrate (C-
51 S-H) phases [6]. They concluded that the Sr^{2+} -binding is mainly a reversible process, with only a small
52 part of the Sr^{2+} being bound in the cement-structure, and that Sr^{2+} is bound to surface sites of C-S-H
53 via bridging oxygen atoms through ion exchange interactions with Ca^{2+} , Na^+ and K^+ on silanol-groups
54 of the C-S-H-phases (in line with an earlier study of Tits et al. (2006) [7]) [6].

55 A promising option for a more effective immobilisation matrix is the use of inorganic polymers (IPs).
56 IPs generally demonstrate a higher fire/acid resistance in comparison to OPC and an increasing
57 number of studies is dedicated to the suitability of IPs for RAW-immobilisation, using a variety of
58 industrial wastes as precursors for the IPs [2,4,8–17]. However, introduced species can have a large
59 impact on the properties of the immobilisation matrix, and this effect has been studied to a much
60 lesser extent [18,19]. Also, the conclusions of these studies are not easily generalized due to high
61 variability in precursor composition, and the differences between high-Ca and low-Ca precursors
62 regarding the IP microstructure and strength development. Provis et al. (2008) studied the effect of

63 caesium and strontium salts (nitrates, sulphates and hydroxides) on metakaolin-based IPs and found
64 that insoluble SrCO_3 formed in all Sr^{2+} -containing samples [18]. They also found that the excess of
65 nitrates precipitates as NaNO_3 and that addition of CsNO_3 caused a clear delaying effect on
66 geopolymer binder formation, being significant even at 0.10 or 0.50 wt% CsNO_3 . In addition, they
67 reported a disruption of the pore structure formation, caused by the presence of ions in the pore
68 solution (particularly the bulky NO_3^-); these anions are repelled by the negatively charged
69 aluminosilicate framework preventing condensation reactions from taking place [18]. This
70 obstruction of gel-hardening was also observed by Komnitsas et al. (2013), who found that the
71 compressive strength of their samples decreased by the presence of NO_3^- and SO_4^- , since these
72 consume part of the alkali activator cations, hindering the geopolymerization reactions [20]. Provis et
73 al. (2008) discussed that Sr^{2+} added as a nitrate will probably behave similarly to Ca^{2+} during
74 geopolymer formation [18]. They noticed a dramatic decrease in the resistivity of the geopolymer
75 binder and attributed this effect to the presence of the nitrate ion, causing a combination of
76 increased pore size and connectivity, and subsequent mobility of the nitrate ions through the
77 solution-filled pores [18]. They didn't observe this effect as strongly in the CsNO_3 -containing samples
78 and attributed this to the lower nitrate concentration [18]. According to Kuenzel et al. (2015), Sr^{2+}
79 uptake in geopolymer activated by a Na^+ -activating solution is limited to 0.4 mol Sr^{2+} per mol of
80 aluminium, and an excess of Sr^{2+} is immobilised by precipitation as hydroxide or carbonate phases
81 [4]. Peng et al. (2016) found that the addition of strontium to metakaolin-zeolite geopolymers caused
82 a hysteresis effect [19]. They attributed the longer setting time to three possible causes: (1)
83 precipitation of Sr^{2+} and OH^- or $[\text{SiO}_4]^{4-}$, passivating the surface of the precursors and slowing down
84 dissolution; (2) reaction of Sr^{2+} and OH^- or $[\text{SiO}_4]^{4-}$ resulting in a decrease in the number of hydroxide-
85 ions and silicon-oxygen tetrahedrons; (3) the introduced ions lower the diffusion rate of all ions
86 present in the system as a function of charge attraction and repulsion, and so postponing the
87 geopolymer gel formation [19]. They also reported that Sr^{2+} takes part in the polymerization reaction
88 and that the Sr^{2+} -ion can replace several Na^+ -ions for charge balancing purposes [19].

89 Fewer studies exist on the use of alkali-activated ground granulated blast furnace slag (GGBFS) for
90 immobilising caesium and strontium in comparison with e.g. alkali-activated metakaolin. According
91 to Gong and White (2016), the primary reaction product in GGBFS-based IPs is a C-(N)-A-S-H gel
92 (calcium-sodium-aluminium-silicate-hydrate), resembling a highly disordered C-S-H [21]. The
93 reported use of IPs based on GGBFS for immobilising Cs⁺ and Sr²⁺ is scarce [2,9]. Qian et al. (2001)
94 prepared GGBFS IPs containing 0.5 wt% Cs⁺ and Sr²⁺ and found them to immobilize Cs⁺ and Sr²⁺ better
95 than an OPC matrix [9]. A similar result was reported by Guangren et al. (2002) [2]. Some authors
96 have added GGBFS as an additive in IPs based on different precursors [14,15,22]. However, the effect
97 of caesium- and strontium-addition on the IP-characteristics is not thoroughly investigated. To fill this
98 existing knowledge gap, IPs based solely on GGBFS and a NaOH activating solution are developed for
99 the immobilisation of Cs⁺ and Sr²⁺. This paper discusses the effect of the introduced species on IP
100 reaction kinetics and physical and mechanical properties.

101 2 Materials and methods

102 Commercially available GGBFS was used as a precursor for the IPs. The slag was first dried at 110 °C
103 to constant weight and then milled for 6 h (Attritor ball mill type 1S, Wiener & Co.). The density of
104 the slag was measured $2.91 \pm 0.01 \text{ g/cm}^3$ (Quantachrome Multipycnometer MVP-6DC). The fineness
105 of the resulting GGBFS powder was measured according to EN 196-6 [23] and found to be 5900 ± 100
106 cm^2/g . The chemical composition of the GGBFS was determined by means of X-ray fluorescence
107 spectroscopy and is shown in **Table 1** (results expressed as oxide, except for Cl).

108 **Table 1:** GGBFS oxide and chloride composition.

Compound	wt%
CaO	42.4
SiO ₂	33.5
Al ₂ O ₃	11.3
MgO	8.5
SO ₃	1.9
TiO ₂	0.7

Na ₂ O	0.4
K ₂ O	0.4
Fe ₂ O ₃	0.4
MnO	0.2
ZrO ₂	0.1
SrO	0.1
Cl	0.1

109

110 IP-pastes were produced by mixing the prepared GGBFS-powder with a 6 mol/L NaOH activating
 111 solution at a liquid-over-solid ratio (L/S) of 0.37, found to be the optimum in an earlier study [24].
 112 The activating solution was prepared from NaOH-pellets (Fischer Scientific, 98.44 % pure) and type II
 113 distilled water. Cs⁺ and Sr²⁺ were added as nitrates (CsNO₃, Alfa Aesar 99.8%; Sr(NO₃)₂, Emsure
 114 99.0%) to account for 0, 0.5, 1 and 2 wt% of the final IP-mass (solid precursor + activating solution +
 115 added nitrates). These amounts were fixed based on literature and earlier experiments (among
 116 which our earlier study [24]). The mixtures were cast in 20 x 20 x 80 mm³ moulds and covered with
 117 plastic foil to prevent dehydration. The hardened samples were demoulded after 1 day, placed in
 118 plastic containers, and allowed to further cure at 21 ± 2 °C for a total curing time of 28 days. The mix
 119 designs are given in Table 2.

120

Table 2: Inorganic polymer mix design (wt%).

	GGBFS	NaOH (6 M)	Cs ⁺	Sr ²⁺	NO ₃ ⁻
IP_0	72.96 ± 0.04	27.04 ± 0.04	-	-	-
IP_Cs_0.5	72.45 ± 0.01	26.81 ± 0.01	0.50 ± 0.01	-	0.23 ± 0.01
IP_Cs_1	71.92 ± 0.01	26.61 ± 0.01	1.00 ± 0.01	-	0.47 ± 0.01
IP_Cs_2	70.87 ± 0.02	26.21 ± 0.01	1.99 ± 0.01	-	0.93 ± 0.01
IP_Sr_0.5	72.12 ± 0.01	26.68 ± 0.01	-	0.49 ± 0.01	0.70 ± 0.01

IP_Sr_1	71.24 ± 0.01	26.36 ± 0.01	-	0.99 ± 0.01	1.41 ± 0.01
IP_Sr_2	69.48 ± 0.02	25.71 ± 0.01	-	1.99 ± 0.01	2.82 ± 0.01

121

122

123 All IPs were characterised for heat release and physical and mechanical properties. Additionally,
 124 morphological and micro-chemical analyses were performed at 28 days of curing. Leaching tests took
 125 place at 48 days of curing. To study the effect of Cs⁺ and Sr²⁺ addition on the heat released during the
 126 alkali activation process, a calorimetric study was performed under isothermal conditions (TAMIII
 127 Thermal Activity Monitor, TA Instruments). A weighed amount of dry precursor was placed in a vial,
 128 while a weighed amount of activating solution was brought into two syringes and placed on top of
 129 the vial. This combination was then inserted into the calorimeter. After a few hours, when the
 130 calorimeter obtained a steady background signal, the activating solution was injected into the vial,
 131 and mixed with the precursor. In this way, the heat release was monitored from the very start of the
 132 reaction.

133 To study morphology and micro-chemistry, a 28-day cured sample of each composition was cut with
 134 a low-speed diamond coated circular saw to 20 x 20 x 5 mm³. This sample was then embedded in
 135 resin, polished, and carbon-coated. The micro-chemical analysis was performed with a Jeol
 136 Hyperprobe field emission gun electron probe micro-analyser (EPMA, JEOL JXA-8530F) equipped with
 137 five wavelength dispersive spectrometers (WDS). In addition to a point-based chemical analysis, the
 138 distribution of caesium and strontium was mapped for each of the samples. The EPMA was operated
 139 at 15 kV and a probe current of 15 nA. For quantitative elemental point analysis, the standards
 140 obsidian (for SiO₂, Na₂O, Al₂O₃), celestite (for SrO), and apatite (for CaO) were used, except for
 141 caesium, where a factory default standard was used instead, due to the unavailability of a known
 142 standard. Mappings for caesium were collected with a dwell time of 40 ms per pixel in an area of 750

143 x 575 pixels (pixel size 0.4 μm), and for strontium with a dwell time of 10 ms per pixel in an area of
144 1300 x 1000 pixels (pixel size 0.8 μm). The mapped surface area for caesium and strontium was 300 x
145 230 μm and 1040 x 800 μm , respectively.

146 The flexural (f_{cf}) and compressive strength (f_c) of the IP-pastes were measured at 1, 8 and 28 days.
147 Of each composition, and at each time of sampling, three samples were used for the flexural
148 strength. The sample dimensions were 20 x 20 x 80 mm^3 . For the compressive strength, six
149 repetitions were performed using cubic samples of 20 x 20 x 20 mm^3 .

150 Determination of water absorption (E_v) (vacuum method), apparent porosity (P), apparent relative
151 density (T), and bulk density (B) were performed following international standard ISO 10545-3 [25].
152 Results showed that the E_v and P were very low (< 1 %), and were not influenced by addition of
153 strontium or caesium. T and B were both measured as $2.1 \pm 0.1 \text{ g/cm}^3$.

154 The capacity for immobilising Cs^+ and Sr^{2+} , and the release of the structural elements were
155 determined by means of a dynamic diffusion test based on the standards ASTM C1220-98 [26] and
156 EN/TS 15863:2015 [27]. IP-subsamples of 20 x 20 x 25 mm^3 were cut from a larger 48-day-cured
157 sample by means of dry cutting (to avoid premature wash-out). These samples were then cleaned
158 using a dry brush, measured for dimensions and weight, and submerged in 400 ml of Milli-Q water
159 while fixed in the centre of the water volume. Both container and sample holder were made of
160 polypropylene. The containers were tightly closed and placed in an oven at $90 \pm 2 \text{ }^\circ\text{C}$ for 7 days. At 1
161 h, 24 h, and 7 d after the start of the leaching experiment, the entire eluate volume was refreshed
162 and aliquots were taken for further characterization. At each sampling time, 10.0 ml of the eluate
163 was filtered over a 0.2 μm syringe filter and acidified immediately after sampling to a concentration
164 of 1 % HNO_3 (MERCK Suprapur 65 %). The concentration of water-soluble Cs^+ was measured by ICP-
165 MS (Perkin Elmer NexION 350S), while the concentrations of Sr^{2+} , Si^{4+} , Al^{3+} , Ca^{2+} , and Na^+ were
166 measured by ICP-OES (Perkin Elmer type Optima 8300). The leaching experiment was performed in
167 twofold for each of the IP-compositions. The results from the ICP-OES and ICP-MS measurements are

168 corrected for dilution and sample surface area. One blanc test per repetition was conducted
169 simultaneously, using 400 ml of Milli-Q water in the exact same conditions, excluding the presence of
170 a sample. The experimental results are expressed as the amount of the element released at sampling
171 time (t), divided by the surface area of the sample (A). The cumulative release of each constituent
172 can be calculated as:

$$R_i = \frac{\sum_0^n [(C_{i,n} - B_{i,n}) \cdot V]}{A} \quad (1)$$

173 With

174 R_i = cumulative release of element i (g/m^2)

175 $C_{i,n}$ = concentration of element i in the filtered aliquot n (g/ml)

176 $B_{i,n}$ = concentration of element i in the filtered blanc aliquot n (g/ml)

177 V = initial volume of eluate in bottle containing sample matrix (ml)

178 A = surface of sample (m^2)

179 Each sample was weighed before and after the leaching experiment. The loss of mass is similar for all
180 samples (between 2 % and 6 %) and does not seem to be affected by the addition of caesium or
181 strontium. At each sampling time, a portion of the eluate was used for measuring pH (calibrated
182 electrode HI1043B, Hanna Instruments) and conductivity (Schott Geräte CG 858, calibrated with 0.1
183 M KCl), while another portion was used for titration purposes, to determine the amount of H^+
184 hydrogen-consuming species released during the leaching process. Titration was performed in
185 threefold using an automated burette (Metrohm Basic Titrino 794) with 0.1 M HCl. The HCl-solution
186 was set with Na_2CO_3 dried at 110 °C as the primary standard.

187 **3 Results and discussion**

188 **Figure 1** shows a visual difference between strontium- and caesium-containing samples. The
189 photographs are taken after 8 days of curing. The white spots observed in the strontium-containing
190 samples are most likely crystals of $\text{Sr}(\text{OH})_2$ (see later section 3.1).



191

192 **Figure 1.** Visual difference between samples containing strontium or caesium. Samples from left to
193 right: IP_0, IP_Cs_0.5, IP_Cs_1, IP_Cs_2, IP_Sr_0.5, IP_Sr_1, IP_Sr_2.

194 3.1 Calorimetry

195 The isothermal calorimetry results are given in **Figure 2**, showing the evolution of the heat released
196 during the alkali activation process of the GGBFS-precursor, and the effect of caesium and strontium
197 additions. The first stage of the reaction is a very fast and exothermic process, reaching a maximum
198 heat flow of about $32 \text{ J h}^{-1} \text{ g}^{-1}$ (per gram of solid precursor) for IP_0. This maximum is reached about
199 50 min after adding the activating solution. The initial heat release is due to sorption of the activating
200 solution on the precursor surface (weathering) and the dissolution of the solid aluminosilicate. After
201 this, a lower but continuous heat release is measured due to ongoing polymerisation reactions [28].
202 The results from **Figure 2** indicate that addition of Cs^+ has little to no effect on the heat released
203 during the alkali activation process. Only a small variation in the maximum heat flow can be observed
204 (peak measurement of $32.2 \text{ J h}^{-1} \text{ g}^{-1}$ for IP_0 and $29.9 \text{ J h}^{-1} \text{ g}^{-1}$ for IP_Cs_2), while no time delay of the
205 maximum takes place. Addition of Sr^{2+} , however, does show a clear effect on the heat flow during the
206 activation process. When increasing the amount of Sr^{2+} , an increasingly distinct peak appears before
207 the initial weathering takes place (e.g. the peak of $25.36 \text{ J h}^{-1} \text{ g}^{-1}$ for IP_Sr_1). This initial peak can be
208 attributed to the formation of $\text{Sr}(\text{OH})_2$ immediately after adding the activating solution to the dry
209 precursor (with $\text{Sr}(\text{NO}_3)_2$ mixed in). This reaction consumes a portion of the hydroxide ions,
210 preventing them to participate in the alkali activation process. This effect would be manifested in a
211 lower heat flow and a horizontal shift (time delay) of the peak (e.g. $21.34 \text{ J h}^{-1} \text{ g}^{-1}$ for IP_Sr_1) to the
212 right. These slower dissolution kinetics are in line with the observed effect of strontium on the
213 setting time of GGBFS IPs reported in an earlier study [24], where it was found that the setting time
214 of a GGBFS-IP-paste is severely delayed by addition of Sr^{2+} . The less profound activation reaction for

215 IP_Sr_1 and IP_Sr_2 (measured as lower heat release, **Figure 2**) also leads to a decreased
216 compressive strength (see section 3.3, **Figure 5**). During the mixing and casting procedure of the IP-
217 samples, the addition of strontium also led to a more viscous mixture.

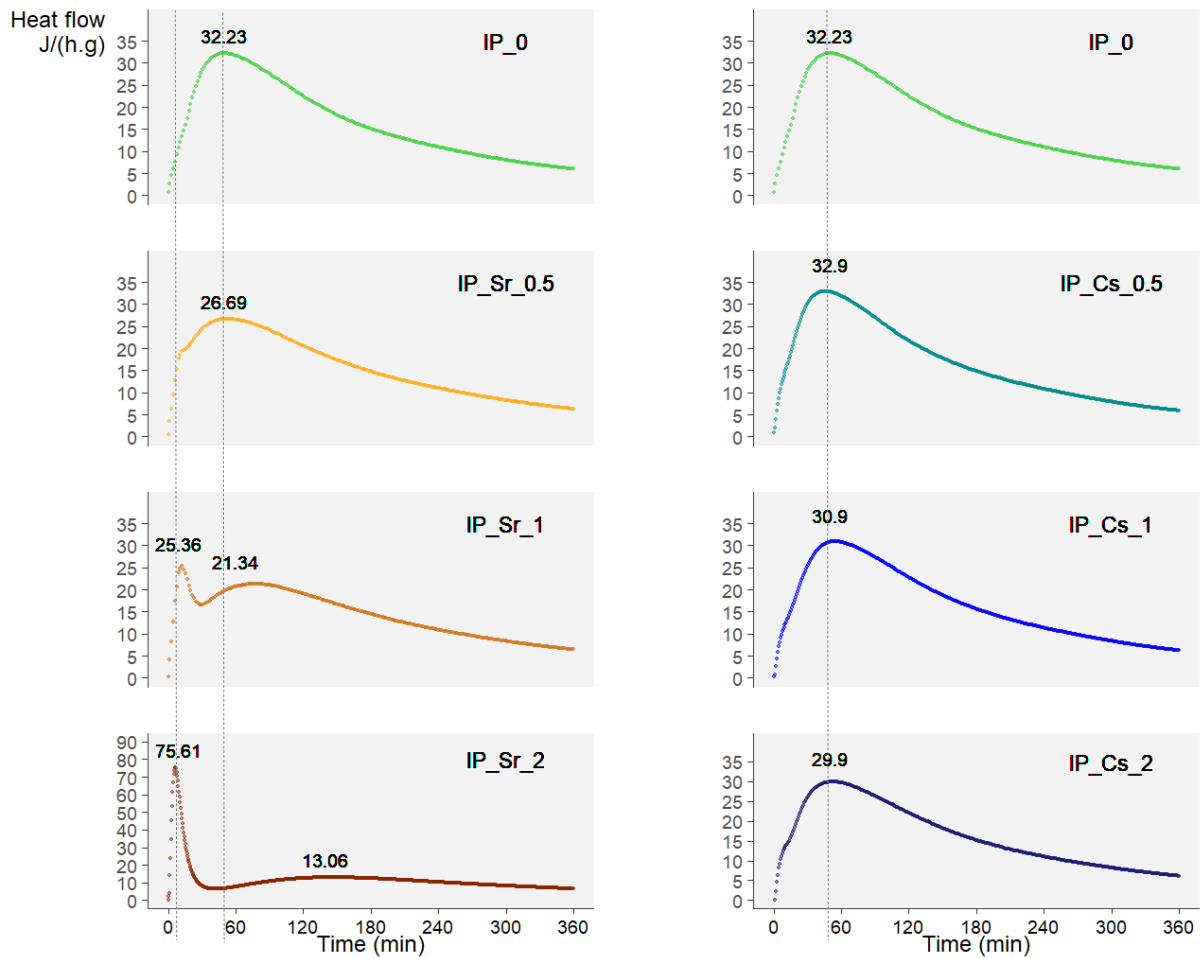
218 It is assumed that strontium hydroxide is formed immediately when Sr^{2+} comes into contact with the
219 activating solution. Equation (2) assumes that the sodium- and nitrate-ions remain dissociated, while
220 equation (3) assumes that the sodium and nitrate will precipitate to form NaNO_3 . The crystallization
221 of NaNO_3 from the pore solution has been reported by Provis et al. (2008) [18] and Blackford et al.
222 (2007) [12] (both metakaolin-based IPs) when adding $\text{Sr}(\text{NO}_3)_2$, although not immediately during
223 mixing, in contrast to the $\text{Sr}(\text{OH})_2$ formation.



224

225 Since the formation of NaNO_3 has been reported to take place during a later drying stage [18], it
226 would thus not cause an immediate energy release during initial mixing. In **Figure 2**, however, for
227 sample IP_Cs_2 a small “shoulder” in the curve is observed; since the amount of nitrates present in
228 this sample is quite high, this could be due to formation of NaNO_3 or the prevention of condensation
229 reactions by the NO_3^- ions as reported by [18,20]. The consumption of hydroxide ions by the
230 introduced strontium reduces the amount available for the activation reaction, which is also
231 reflected in the decreased OH-leaching in the strontium-containing samples (later section 3.4.4,
232 **Figure 12**). The white spots observed in the strontium-containing samples (see **Figure 1**) are most
233 likely regions of $\text{Sr}(\text{OH})_2$, which precipitate as a fine white crystalline solid.

234



235

236

Figure 2: Effect of adding Sr^{2+} and Cs^+ on the heat released per gram of solid precursor ($\text{J h}^{-1} \text{g}^{-1}$)

237

during alkali activation of GGBFS.

238

3.2 Micro-chemical analysis

239

The results from the WDS micro-chemical analyses on the IP-samples are shown in **Table 3**. It is

240

important to note that the amounts given in **Table 3** are weight-percentages of the IP-matrix formed

241

by the activation process, excluding the undissolved precursor particles (hereafter referred to as

242

matrix), and not of the total IP-mass (hereafter referred to as IP_m). The fractions of introduced

243

strontium and caesium that are incorporated into the matrix, taking into account the ratio of formed

244

matrix over undissolved precursor, are determined by the following approach: using *Particle (Pores)*

245

and *Cracks Analysis System (PCAS)* software, a number of images were separately analysed to

246

average the surface ratios of matrix over undissolved precursor, which was found to be about 65/35.

247 Since this ratio is obtained using different images of randomly cut samples, it can also be assumed
 248 valid as a volume over volume ratio. Using this ratio, the density of the matrix phase is found to be
 249 1.7 g/cm³, calculated using equation (4). The matrix phase, and the calculated density include
 250 possible pores and cracks. But since the open porosity is very low (see section 2), this influence is
 251 expected to be limited. The measured amounts of caesium and strontium (**Table 3**) in the matrix are
 252 converted to their respective fractions in the total IP-sample using equation (5).

$$\rho_M = \frac{\rho_{IP_m} - 0.35 * \rho_{GGBFS}}{0.65} \quad (4)$$

$$wt\%_{IP_m} = \frac{wt\%_M * 0.65 * \rho_M}{\rho_{IP_m}} \quad (5)$$

253

254 With

255 ρ_M = density of the matrix (g/cm³)

256 ρ_{IP_m} = density of the total inorganic polymer sample (2.1 g/cm³, see section 2)

257 ρ_{GGBFS} = density of the GGBFS precursor (2.91 g/cm³, see section 2)

258 $wt\%_{IP_m}$ = weight-percentage of Cs⁺ or Sr²⁺ in the total inorganic polymer sample

259 $wt\%_M$ = weight-percentage of Cs⁺ or Sr²⁺ in the matrix phase (as tabulated in **Table 3**)

260

261 For each measured $wt\%_M$, the calculated $wt\%_{IP_m}$ is given in **Table 4**, together with the fractions of
 262 the introduced caesium and strontium that are incorporated in the matrix ($wt\%_{IP_m}$ divided by 0.5, 1
 263 or 2 wt%, multiplied by 100 %). Because of the uncertainty in the 65/35 ratio, the values in **Table 4**
 264 are given as estimates. From these values it can be deduced that for caesium, about all of the
 265 introduced Cs⁺ is incorporated into the IP-matrix. These findings are in line with the study of
 266 Blackford et al. (2007), who reported that Cs⁺ is fully incorporated at the nm-scale into the
 267 amorphous geopolymer phase [12]. For Sr²⁺, the amounts shown in **Table 4** are corrected for the
 268 initial strontium-content measured in IP_0; the tabulated wt% are thus the amounts of Sr²⁺

269 incorporated in the IP-matrix in addition to the inherent strontium from the precursor. From these
 270 results it can be concluded that in every step of strontium addition (0.5, 1, and 2 wt%), about one
 271 sixth is incorporated into the IP-matrix. Results from **Table 3** indicate that addition of strontium or
 272 caesium has no effect on the amounts of silicon, aluminium and sodium in the matrix. However, a
 273 small effect on the amount of calcium is observed. Adding caesium seems to cause a slight decrease
 274 of the Ca²⁺-content, possibly caused by Cs⁺ replacing Ca²⁺, since Ca²⁺ can act as a charge balancing
 275 ion [29].

276 **Table 3:** Results of micro-chemical analysis using EPMA (calculated from oxides).

Element (wt%)	IP_0	IP_Sr_0.5	IP_Sr_1	IP_Sr_2
Si ⁴⁺	13 ± 1	13 ± 1	12.6 ± 0.6	13 ± 1
Al ³⁺	5.3 ± 0.3	6 ± 1	5.5 ± 0.3	6.1 ± 0.6
Ca ²⁺	16.2 ± 0.9	17 ± 2	17 ± 1	17 ± 2
Na ⁺	2.0 ± 0.6	1.9 ± 0.5	2.6 ± 0.7	2.5 ± 0.4
Sr ²⁺	0.20 ± 0.02	0.36 ± 0.01	0.47 ± 0.09	0.9 ± 0.1
Cs ⁺	-	-	-	-
Element (wt%)		IP_Cs_0.5	IP_Cs_1	IP_Cs_2
Si ⁴⁺		13 ± 1	13 ± 1	12.5 ± 0.9
Al ³⁺		6.2 ± 0.6	5.8 ± 0.7	5.7 ± 0.8
Ca ²⁺		12 ± 2	13 ± 1	12.8 ± 0.7
Na ⁺		3.6 ± 0.4	2.5 ± 0.8	2.9 ± 0.4
Sr ²⁺		0.19 ± 0.02	0.19 ± 0.03	0.19 ± 0.02
Cs ⁺		1.32 ± 0.09	1.8 ± 0.4	3.6 ± 0.4

277

278

279

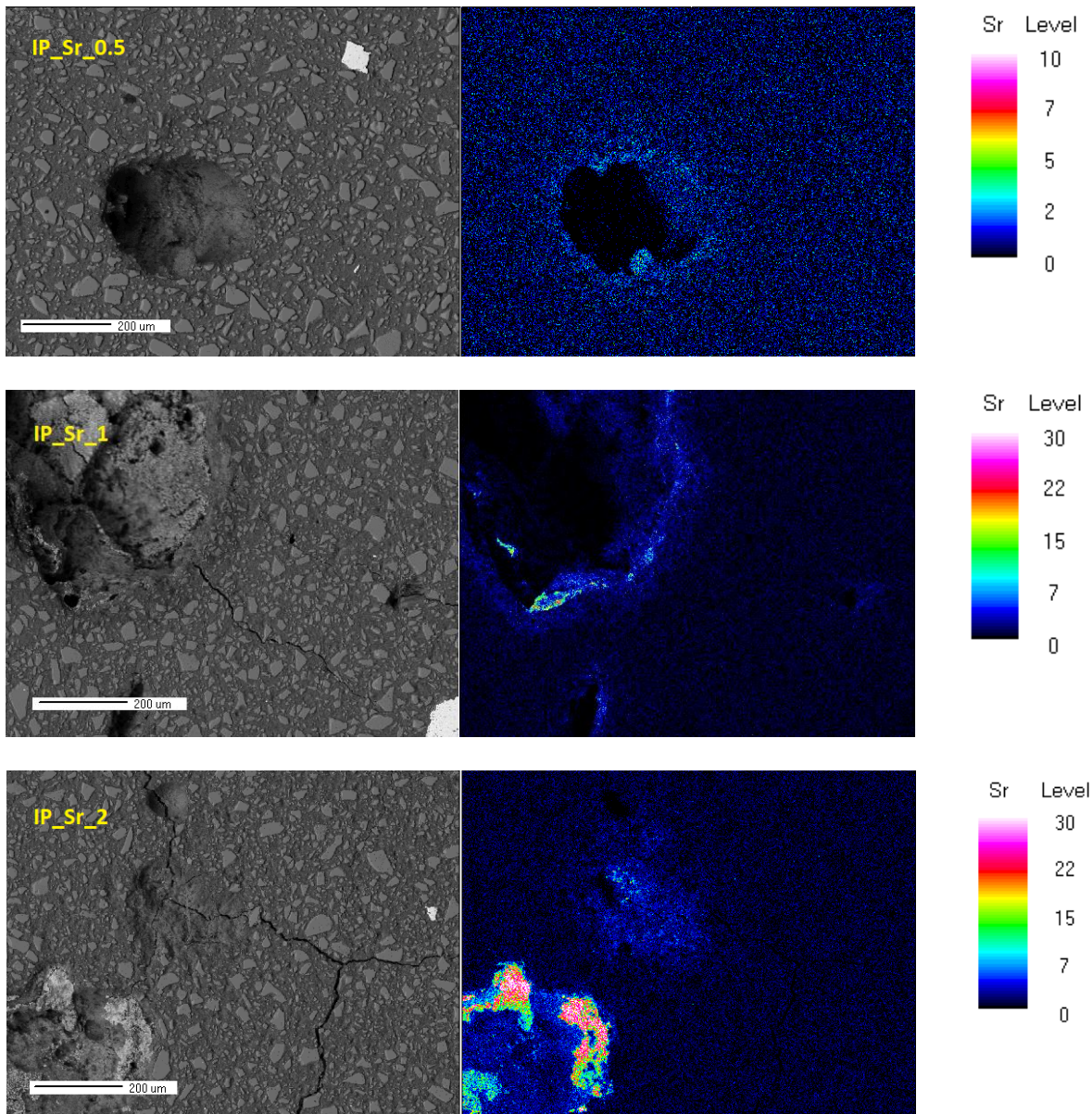
280 **Table 4.** (a) Weight-percentages of caesium and strontium incorporated in the matrix phase,
 281 recalculated for the entire IP-mass, and corrected for initial strontium content. (b) Percentages of
 282 introduced caesium and strontium that are incorporated into the matrix.

(a) wt% _{IP_{M,cor}}	IP_Sr_0.5	IP_Sr_1	IP_Sr_2	IP_Cs_0.5	IP_Cs_1	IP_Cs_2
Sr ²⁺	0.08	0.14	0.36	-	-	-
Cs ⁺	-	-	-	0.68	0.93	1.86
(b) Fraction incorporated into matrix (%)						
Sr ²⁺	17	14	18	-	-	-
Cs ⁺	-	-	-	100*	93	93

* This value is rounded down since the calculated value is 137 % (probably due to statistical variation in the concentrations at the measurement points)

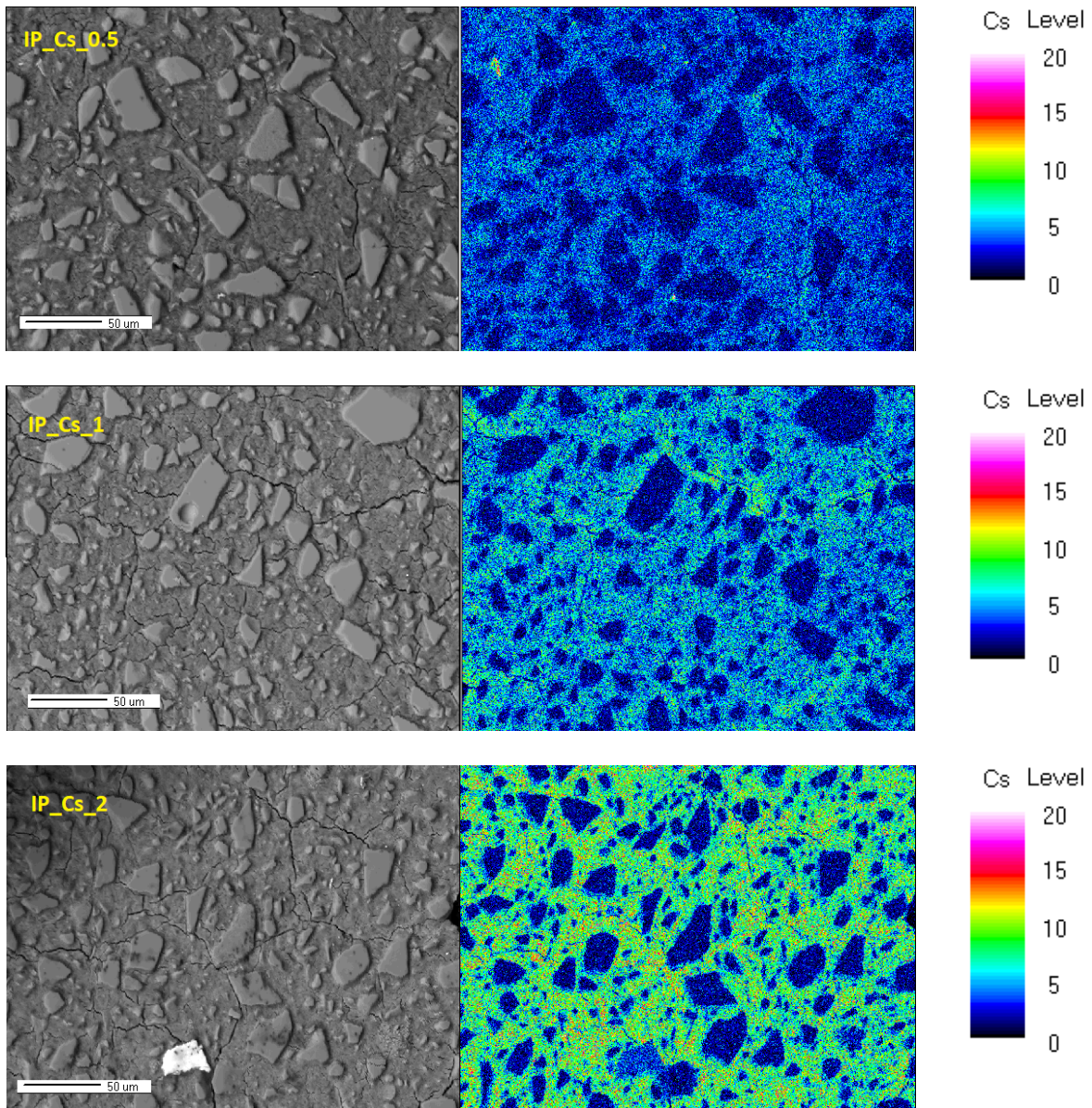
283

284 **Figure 3** and **Figure 4** show mappings of these same samples to study the distribution of caesium and
 285 strontium throughout the microstructure. Mapping of the Sr²⁺-containing samples is done at a larger
 286 scale than for the Cs⁺-samples because this allows a clear view of precipitation sites for Sr(OH)₂, while
 287 the smaller scale for the Cs-samples allows a clearer view of the incorporation of Cs⁺ in the binder.
 288 For the samples containing added strontium, precipitation sites are clearly visible where large
 289 amounts of strontium are concentrated. From **Figure 3**, sample IP_Sr_0.5, it can be observed that a
 290 small amount of strontium is distributed evenly throughout the microstructure. **Figure 3** also shows
 291 large pores where the Sr²⁺ seems to be concentrated. **Figure 4** shows that Cs⁺ is incorporated
 292 homogeneously throughout the binder-phase. This difference in incorporation is also reflected in the
 293 leaching results (see further, section 3.4), where Cs⁺ leaches out more easily since it is distributed
 294 evenly throughout the structure (and thus being more available at the sample surface), while Sr²⁺ is
 295 more physically encapsulated (and thus less available at the sample surface).



296 **Figure 3:** EPMA mappings of IP_Sr_0.5, IP_Sr_1 and IP_Sr_2. The level-scale of IP_Sr_0.5 is smaller for
 297 improved visibility of the distribution of strontium throughout the matrix. The chemical composition
 298 of the samples is given in **Table 3**.

299

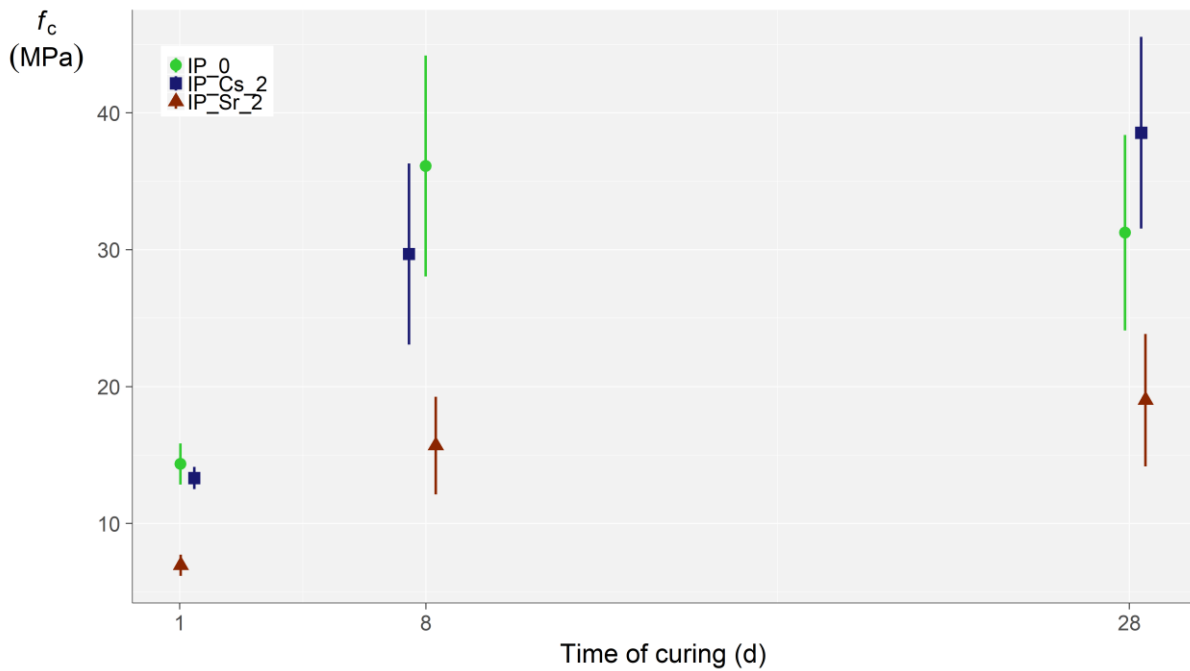


300 **Figure 4:** EPMA mappings of IP_Cs_0.5, IP_Cs_1 and IP_Cs_2. The chemical composition of the
 301 samples is given in **Table 3**.

302 *3.3 Compressive and flexural strength*

303 The compressive strength data shown in **Figure 5** indicate that addition of CsNO₃ does not
 304 significantly affect the strength development. Addition of Sr(NO₃)₂, however, does show a
 305 deleterious effect on the compressive strength. After 1 day and 8 days of curing, the compressive
 306 strength of IP_Sr_2 is only about 45 % of the values for IP_0. This difference is reduced with
 307 increased curing time. At 28 days of curing, IP_Sr_2 (19 ± 5 MPa) reaches about 60 % of the

308 compressive strength of IP_0 (31 ± 7 MPa). This negative effect on the compressive strength is
309 probably caused by the less profound alkali activation reaction due to the formation of $\text{Sr}(\text{OH})_2$ and
310 NaNO_3 , causing a less concentrated activating solution and resulting in slower dissolution kinetics (as
311 discussed in section 3.1, and observed in an earlier study [24] as a longer setting time). The
312 occurrence of $\text{Sr}(\text{OH})_2$ precipitation spots and accompanying pores (see **Figure 1** and **Figure 3**) can
313 also cause weak spots in the IP-structure. Provis et al. (2008) found that, in a metakaolin-based
314 system, the addition of CsNO_3 caused a clear delaying effect on geopolymer gel formation, being
315 significant even at 0.10 or 0.50 wt% CsNO_3 , and attributed this to the presence of NO_3^- [18]. Since no
316 negative effect is observed in the caesium-containing samples in this study, the decrease in
317 compressive strength for the strontium-containing samples cannot be attributed to the presence of
318 nitrates, but rather the presence of Sr^{2+} . A similar conclusion can also be drawn from an earlier study
319 [24] where it was found that adding up to 2 wt% Cs^+ (in the form of nitrates) only showed a small
320 effect on the final setting time (delay of up to 40 %), while strontium-addition retarded final setting
321 severely (delay of 140 % at 0.5 wt% Sr^{2+}). For the flexural strength of the samples, the standard
322 deviations are much too high to distinguish clearly between the results. Only at 1 day and 8 days of
323 curing, there is a small discernible difference between IP_0 (1d: 9 ± 1 MPa; 8d: 12 ± 1) and IP_Sr_2
324 (1d: 7 ± 1 MPa; 8d: 9 ± 2 MPa). At 28 days of curing, no significant difference was observed.



325

326 **Figure 5:** Compressive strength of IP_0, IP_Sr_2 and IP-Cs_2. Measurement points have been

327 randomly offset from the times of curing (1 d, 8 d, and 28 d) for increased discernibility.

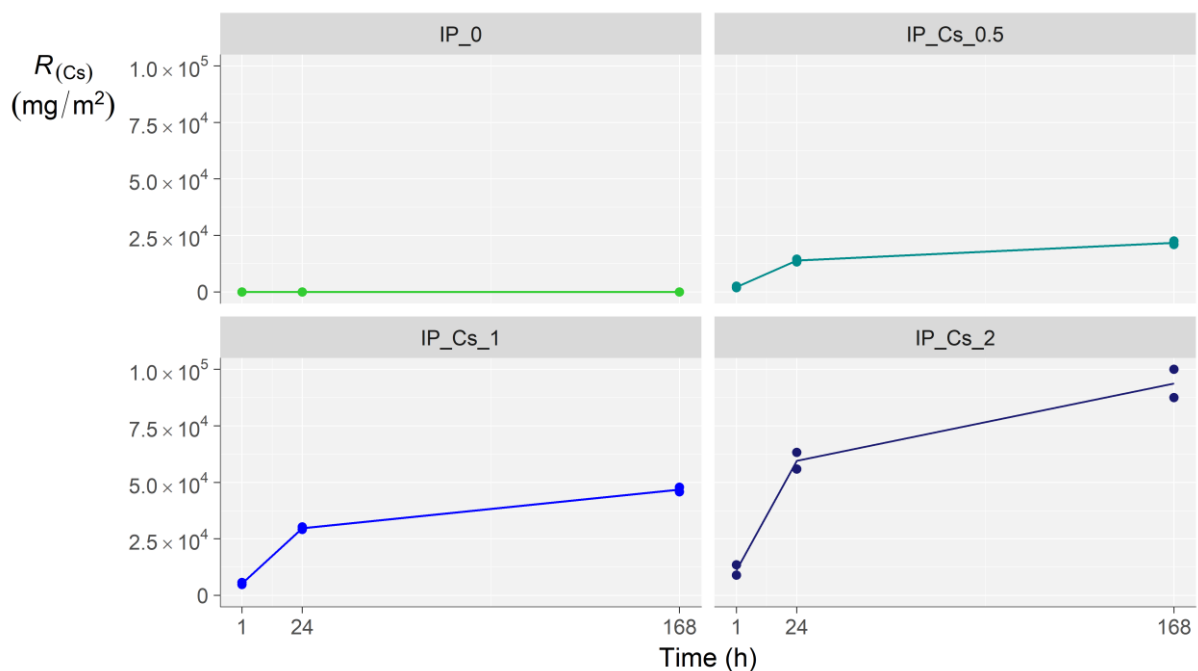
328 *3.4 Leaching of structural and added elements*

329 By use of a dynamic accelerated leaching test, the amount of Cs⁺, Sr²⁺, and structural elements
 330 released has been studied. For the release of caesium and strontium, only results are shown from the
 331 samples where the respective elements were added, together with IP_0. Overall, the measurement
 332 points lie very close together.

333 *3.4.1 Release of Cs⁺*

334 The results of IP-Cs_0.5, IP-Cs_1 and IP-Cs_2 (**Figure 6**) show that the amount of Cs⁺ released
 335 increases proportionally with the amount of Cs⁺ introduced in the IP-matrix. There is no obvious
 336 change in leaching behaviour when adding more Cs⁺, only an increase in the total amount released.
 337 When taking into account the amount of Cs⁺ introduced into each sample, the mass of the sample,
 338 and the total amount of Cs⁺ leached out, the percentage of introduced Cs⁺ that was released can be
 339 determined. For IP-Cs_0.5, IP-Cs_1, and IP-Cs_2 this is respectively 63 %, 66 %, and 62 %. This

340 finding is in line with the proportional caesium-incorporation in the IP-binder, discussed in paragraph
341 3.2.

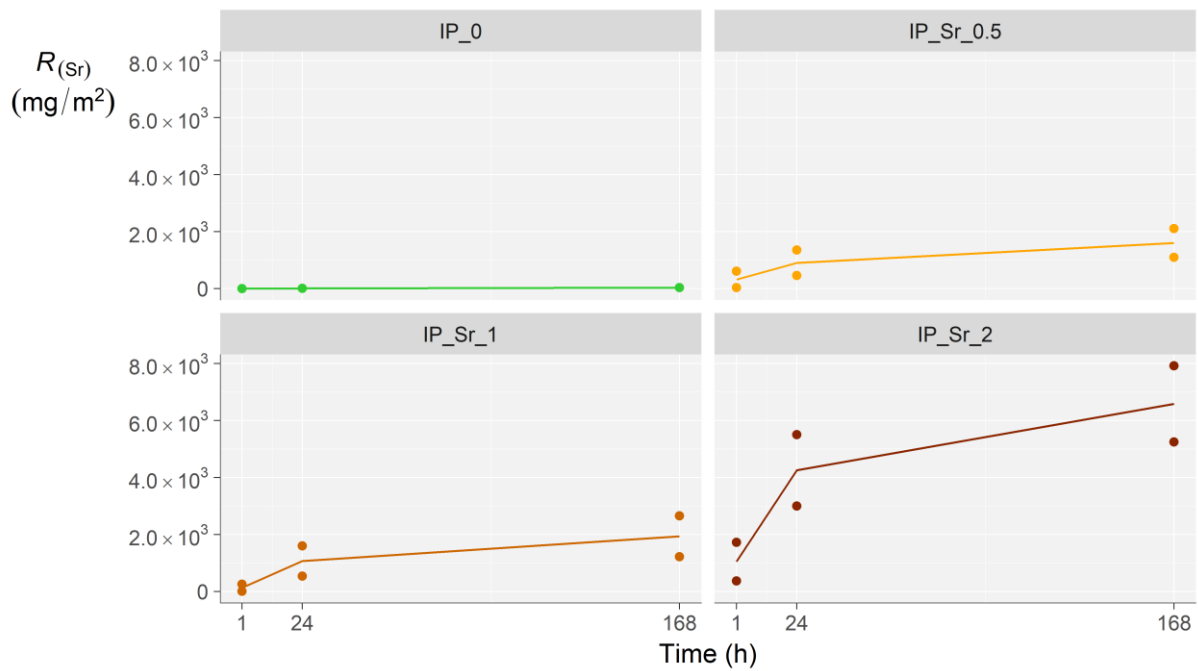


342

343 **Figure 6:** Cumulative release of Cs^+ during a 7-day dynamic leaching test.

344 3.4.2 Release of Sr^{2+}

345 A small amount of Sr^{2+} , present in the GGBFS, leaches out from the base sample IP_0 (about 35
346 mg/m^2 after 7 days). When adding increasing amounts of Sr^{2+} , a proportional increase in Sr^{2+} -release
347 is not immediately observed (see **Figure 7**). The measurement results are also less precise than the
348 results for the other elements. This is most likely due to the fact that a large part of the Sr^{2+} is
349 precipitated in the IP-structure as $Sr(OH)_2$ (as discussed in sections 3.1 and 3.2). This causes a
350 distribution of precipitation sites (see **Figure 1**). Due to the casting process and cutting of the
351 samples into smaller subsamples, a variation occurs in the amount of precipitated $Sr(OH)_2$ spots on or
352 near the surface of the samples. This causes a variation in the amount of $Sr(OH)_2$ available for
353 immediate dissolution from these precipitation spots. The amounts of introduced Sr^{2+} that were
354 released, are 3 %, 2 %, and 4 % for IP_Sr_0.5, IP_Sr_1, and IP_Sr_2 respectively.



355

356

Figure 7: Cumulative release of Sr²⁺ during a 7-day dynamic leaching test.

357

3.4.3 Release of structural elements

358

Figure 8 and **Figure 9** show the cumulative release of Al³⁺, Si⁴⁺, Ca²⁺ and Na⁺ respectively. Al³⁺-release

359

of about 2000 mg/m² for IP_0, IP_Cs_0.5, IP_Cs_1 and IP_Cs_2 is observed. Addition of Cs⁺ to the

360

base IP does not seem to affect the leaching of Al³⁺ from the IP-matrix. Addition of Sr²⁺, however,

361

does show a decrease in the amount of Al³⁺ released during leaching, dropping to a value of about

362

1400 mg/m² for IP_Sr_2. The reason for this is unclear. **Figure 8** shows cumulative Si⁴⁺-release of

363

about 1750 mg/m² for all samples. Addition of Cs⁺ or Sr²⁺ does not seem to have any effect on the

364

amount of Si⁴⁺ released. Cumulative Ca²⁺-release of about 5000 mg/m² is reached for IP_0, IP_Cs_0.5,

365

IP_Cs_1 and IP_Cs_2. Addition of Cs⁺ to the base IP does not seem to affect the leaching of Ca²⁺ from

366

the IP-matrix. Addition of Sr²⁺, however, does show a slight increase in the amount of Ca²⁺ released

367

during leaching, rising to a value of about 6500 mg/m². A possible explanation for this is that the

368

added Sr²⁺ can replace Ca²⁺ as a charge-balancing ion, since Sr²⁺ can behave similarly to Ca²⁺ during IP

369

formation [18]. Also, since high-calcium GGBFS precursors give rise to calcium-(aluminium)-silicate-

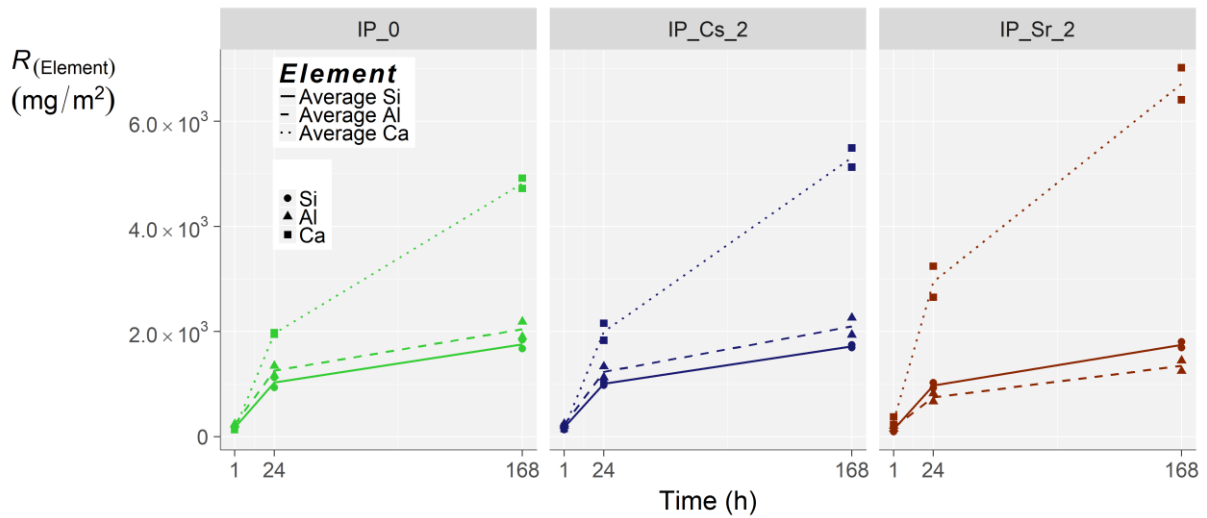
370

hydrate (C-(A)-S-H) formation [21], it could be that Sr²⁺ replaces Ca²⁺ in the C-S-H, giving rise to a C-

371

(Sr)-A-S-H phase. This is in line with the findings of Wieland et al. (2008) and Tits et al. (2006), where

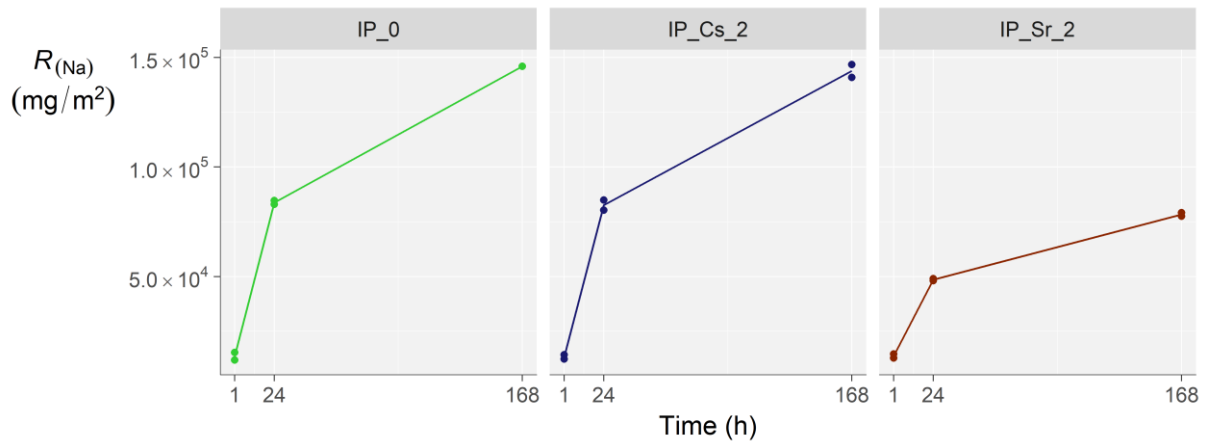
372 strontium-uptake in cementitious materials occurred through ion exchange with Ca^{2+} on silanol-
373 groups of the C-S-H-phases [6,7]. Both options would result in a structure where Ca^{2+} is less strongly
374 bound in the microstructure. This can also be seen in section 3.2, **Table 3** where the amount of Ca^{2+}
375 measured in the IP-matrix decreases slightly when adding more Sr^{2+} . **Figure 9** shows cumulative Na^+ -
376 release of about $1.5 \times 10^5 \text{ mg/m}^2$ for IP_0 and IP_Cs_2. Addition of Sr^{2+} seems to cause a significant
377 decrease in the amount of Na^+ released during leaching, dropping to a value of about 7.5×10^4
378 mg/m^2 for IP_Sr_2, which is half of the Na^+ -release from IP_0. This could be caused by the formation
379 of NaNO_3 as discussed in section 3.1, and further elaborated in the next section (3.4.4). The
380 formation of NaNO_3 seems to be a plausible cause, since Kuenzel et al. (2015) observed an increase
381 in Na^+ -leaching when adding strontium in the form of $\text{Sr}(\text{OH})_2$ to their IP-mixture (and thus having no
382 nitrates in their samples) [4]. Since the EPMA measurements (see section 3.2, **Table 3**) do not
383 indicate a difference in Na^+ content in the IP-matrix, it can be deduced that the formation of NaNO_3
384 occurs after 28 days (EPMA was performed on 28-day-cured samples, while leaching was performed
385 on 48-day-cured samples). Since the samples for the leaching test were cut and transported in
386 ambient conditions, it is also likely that some drying occurred, increasing the formation of NaNO_3 (as
387 mentioned by Provis et al. (2008) that NaNO_3 crystallization from the pore solution could occur
388 during drying of the sample [18]). Addition of Cs^+ to the base IP does not seem to affect the leaching
389 of Na^+ from the IP-matrix. This indicates that adding CsNO_3 does not cause the formation of NaNO_3 .
390 The latter was also reported by Blackford et al. (2007), who observed no formation of NaNO_3 when
391 adding CsNO_3 , while $\text{Sr}(\text{NO}_3)_2$ addition did cause NaNO_3 crystallization [12].



392

393

Figure 8: Cumulative release of Si⁴⁺, Al³⁺, and Ca²⁺ during a 7-day dynamic leaching test.



394

395

Figure 9: Cumulative release of Na⁺ during a 7-day dynamic leaching test.

396 3.4.4 Characterizing eluate

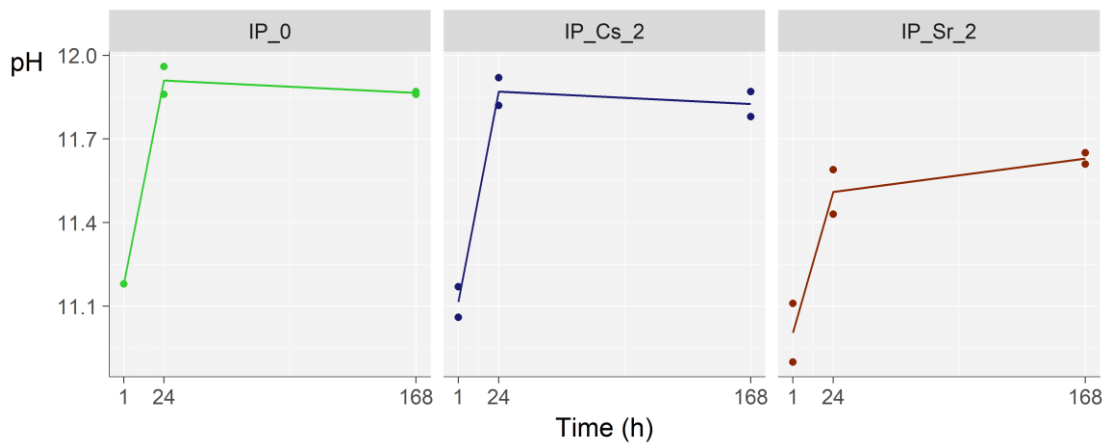
397 **Figure 10** shows the measured pH-values of the eluate at different sampling times (1 h, 24 h, and 168
 398 h after start leaching). These results show that the addition of caesium to the base IP-mixture does
 399 not have a significant effect on the pH of the eluate. Adding strontium, however, does show an
 400 influence on the pH of the eluate, decreasing gradually with increasing amounts of strontium (from
 401 pH 11.9 for IP_0 to pH 11.6 for IP_Sr_2). This decrease in pH is to be expected when Sr(OH)₂ is
 402 formed, trapping part of the introduced hydroxides in the IP-structure, and thus preventing them
 403 from leaching out. Regarding the conductivity of the eluate (**Figure 11**), the addition of caesium to

404 the base IP-mixture again doesn't show any significant change, while a clear change is observed
405 when adding strontium. When adding 2 wt% of strontium to the base IP-mixture, a drop to about
406 half is observed in the conductivity of the eluate (at 24 h and 168 h after the start of the leaching
407 test). Taking into account the measured ions in the eluate (section 3.4), this change in conductivity
408 seems most likely to be the cause of the lower Na⁺-leaching in the strontium-containing samples.
409 However, since the conductivity is also influenced by other charged species, the amount of
410 hydrogen-consuming ions released in the eluate is also determined by use of automatic titration.

411 **Figure 12** shows the results of the titration tests. During titration, 3 equivalence points were
412 measured (around pH 10, pH 8.5, and pH 5). The positions of these equivalence points did not
413 depend on the sampling time of the leaching test (1 h, 24 h, 168 h). The presence of these three
414 equivalence points indicates that other hydrogen-consuming species (besides hydroxides) are
415 present in the eluate. When comparing the results in **Figure 12** from the base IP-mixture (IP_0) and
416 the caesium containing samples (IP_Cs_0.5, IP_Cs_1, and IP_Cs_2), no clear difference is observed in
417 the amount of H⁺-ions necessary to reach equivalence, and thus in the release of hydrogen-
418 consuming species during leaching. The results from the strontium-containing samples (IP_Sr_0.5,
419 IP_Sr_1, and IP_Sr_2), however, do show an effect on the amount of H⁺-ions necessary for
420 equivalence. After 1 h of leaching a small difference is already visible for IP_Sr_1 and IP_Sr_2. At the
421 24 h and 168 h sampling times, this difference has increased, indicating that the eluate from e.g.
422 IP_Sr_2 contains about half the amount of hydrogen-consuming species compared to the eluate of
423 IP_0. The number of hydroxide-ions released, calculated from the measured pH-values, is 37 ± 2 % of
424 the amount of total hydrogen-consuming species (see **Figure 12**) for all samples over the total
425 leaching period, leaving about 60 % for other unidentified hydrogen-consuming species.

426 Calculated from the measured pH-values, the eluates of IP_Sr_0.5, IP_Sr_1 and IP_Sr_2 contain
427 respectively about 17 %, 40 % and 50 % less hydroxide-ions than the eluate of IP_0. The trend
428 observed when adding increasing amounts of strontium to the base mixture is similar for the

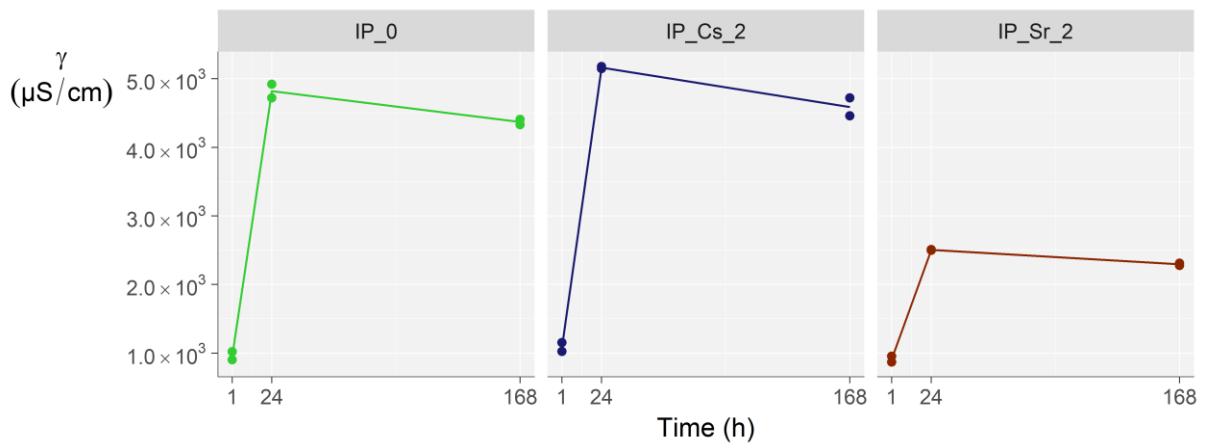
429 measured Na^+ -concentration, conductivity, and OH^- -concentration. Results for all three parameters
 430 seem to drop slightly when adding 0.5 wt% strontium, while dropping by about 35-40 % and 50 %
 431 when adding 1 and 2 wt% respectively. From this, it can be concluded that the amounts of OH^- and
 432 Na^+ released during leaching are closely linked, and affected similarly when adding strontium. A first
 433 possible explanation for the lower release of both OH^- and Na^+ when adding increasing amounts of
 434 strontium can be that strontium hydroxide is formed immediately when Sr^{2+} comes into contact with
 435 the activating solution (see section 3.1). Since the positive Sr^{2+} -ions are consumed by the hydroxide-
 436 ions, the remaining NO_3^- -anions could cause the Na^+ -cations to be more strongly retained due to
 437 ionic interaction or NaNO_3 precipitation. The possible interactions between strontium, sodium and
 438 hydroxide are shown as equations (2) and (3).



439

440

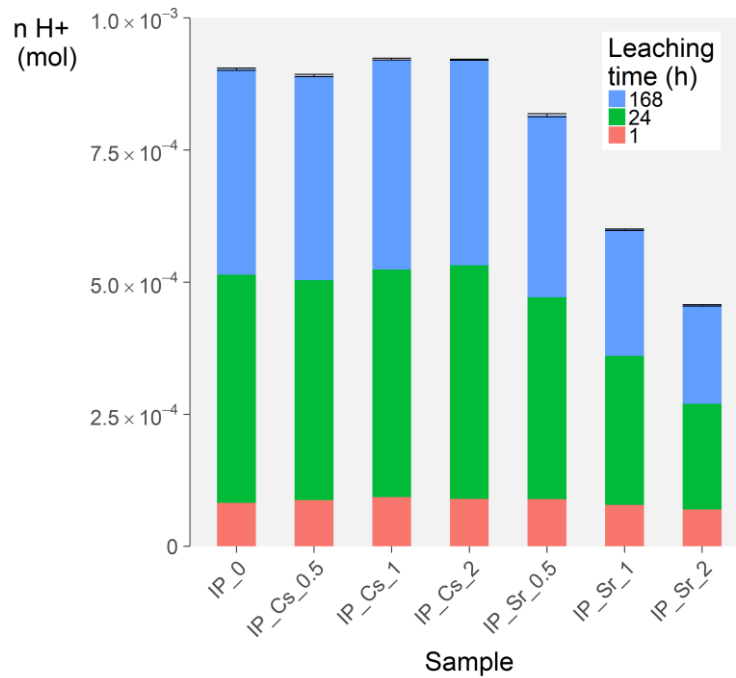
Figure 10: pH-values of eluates at different sampling times.



441

442

Figure 11: Conductivity γ ($\mu\text{S}/\text{cm}$) of eluates at different sampling times.



443

444 **Figure 12:** Cumulative amounts of H^+ -ions added to neutralize the eluate (covering three equivalence
445 points of $\text{pH} \approx 10$, $\text{pH} \approx 8.5$, and $\text{pH} \approx 5$).

446 4 Conclusion

447 In this paper, the effect of adding Sr^{2+} and Cs^+ to a GGBFS-based IP was discussed. Sr^{2+} and Cs^+ were
448 added, as nitrates, to a base IP-mixture to account for 0.5, 1, and 2 wt% of the final IP-mass.
449 Calorimetric results indicate that Cs^+ did not show any significant effect on the early reaction kinetics.
450 Sr^{2+} , however, severely affected the reaction kinetics by forming $\text{Sr}(\text{OH})_2$ immediately after
451 introducing the activating solution to the dry precursor. This consumed part of the available
452 hydroxides resulting in a reduced dissolution of the precursor and thus a reduced polymerization
453 reaction. This is also visible in the lower compressive and flexural strength. The micro-chemical
454 analysis shows that almost all of the introduced Cs^+ is incorporated in the IP-matrix, while only about
455 one-sixth of the introduced Sr^{2+} is incorporated into the matrix phase. It was also observed that
456 adding caesium caused a decrease in the Ca^{2+} -content in the IP-matrix. Water absorption

457 experiments show that water absorption and apparent porosity of the samples is very low, and not
458 significantly affected by the addition of caesium or strontium. From the leaching experiments, results
459 show that Cs^+ -leaching is proportional to the amount of Cs^+ added. For all caesium-containing
460 samples, the final amount of Cs^+ released were all around 65 % of the introduced amount. The total
461 Sr^{2+} -release was around 3 % of the introduced amount for each strontium-containing sample.
462 Strontium-addition resulted in an increased Ca^{2+} -leaching while causing a significant decrease in the
463 amount of Na^+ and OH^- leached. In general, the addition of Cs^+ did not show any significant effect on
464 the studied parameters. Adding Sr^{2+} , however, caused an important decrease in the number of
465 hydroxides available for the dissolution of the precursor resulting in a lower overall strength. For
466 IP_Sr_0.5, the 1-day and 28-day compressive strength show no significant decrease compared to
467 IP_0. Since the addition of 0.5 wt% Sr^{2+} results in a delayed setting time of 140 % in addition to the
468 base sample[24][24][24][24], the application of strontium as a retarder in inorganic polymer
469 development seems very promising. In future work, optimisation of the IP-composition for improved
470 Cs^+ and Sr^{2+} immobilisation will be studied.

471 **Acknowledgements**

472 The authors would like to thank the research group of Applied and Analytical Chemistry (TANC) of
473 Hasselt University for the ICP-OES and ICP-MS measurements. The authors would also like to thank
474 the research group of Physical Chemistry and Polymer Science of the Vrije Universiteit Brussel (VUB),
475 and in particular Prof. dr. ir. Hubert Rahier and ir. Antigoni Katsiki, for the calorimetric
476 measurements.

477 **References**

- 478 [1] International Atomic Energy Agency, The behaviours of cementitious materials in long term
479 storage and disposal of radioactive waste : results of a coordinated research project, Vienna,
480 2013.
- 481 [2] Q. Guangren, L. Yuxiang, Y. Facheng, S. Rongming, Improvement of metakaolin on radioactive

- 482 Sr and Cs immobilization of alkali-activated slag matrix, *J. Hazard. Mater.* 92 (2002) 289–300.
483 doi:10.1016/S0304-3894(02)00022-5.
- 484 [3] M. Ochs, D. Mallants, L. Wang, *Radionuclide and Metal Sorption on Cement and Concrete*,
485 Springer International Publishing, 2016. doi:10.1007/978-3-319-23651-3.
- 486 [4] C. Kuenzel, J.F. Cisneros, T.P. Neville, L. Vandeperre, S.J.R. Simons, J. Bensted, C.R.
487 Cheeseman, Encapsulation of Cs/Sr contaminated clinoptilolite geopolymers produced from
488 metakaolin, *J. Nucl. Mater.* 466 (2015) 94–99.
- 489 [5] S. Goni, A. Guerrero, M.P. Lorenzo, Efficiency of fly ash belite cement and zeolite matrices for
490 immobilizing cesium, *J. Hazard. Mater.* 137 (2006) 1608–1617.
491 doi:10.1016/j.jhazmat.2006.04.059.
- 492 [6] E. Wieland, J. Tits, D. Kunz, R. Dähn, Strontium Uptake By Cementitious Materials, *Environ. Sci.*
493 *Technol.* 42 (2008) 403–409.
- 494 [7] J. Tits, E. Wieland, C.J. Müller, C. Landesman, M.H. Bradbury, Strontium binding by calcium
495 silicate hydrates, *J. Colloid Interface Sci.* 300 (2006) 78–87. doi:10.1016/j.jcis.2006.03.043.
- 496 [8] M.Y. Khalil, E. Merz, Immobilization of intermediate-level wastes in geopolymers, *J. Nucl.*
497 *Mater.* 211 (1994) 141–148. doi:10.1016/0022-3115(94)90364-6.
- 498 [9] G. Qian, D.D. Sun, J.H. Tay, New aluminium-rich alkali slag matrix with clay minerals for
499 immobilizing simulated radioactive Sr and Cs waste, *J. Nucl. Mater.* 299 (2001) 199–204.
500 doi:10.1016/S0022-3115(01)00700-0.
- 501 [10] A. Fernandez-Jimenez, D.E. MacPhee, E.E. Lachowski, A. Palomo, Immobilization of cesium in
502 alkaline activated fly ash matrix, *J. Nucl. Mater.* 346 (2005) 185–193.
503 doi:10.1016/j.jnucmat.2005.06.006.
- 504 [11] C. Shi, a. Fernández-Jiménez, Stabilization/solidification of hazardous and radioactive wastes
505 with alkali-activated cements, *J. Hazard. Mater.* 137 (2006) 1656–1663.
506 doi:10.1016/j.jhazmat.2006.05.008.
- 507 [12] M.G. Blackford, J. V. Hanna, K.J. Pike, E.R. Vance, D.S. Perera, Transmission electron
508 microscopy and nuclear magnetic resonance studies of geopolymers for radioactive waste
509 immobilization, *J. Am. Ceram. Soc.* 90 (2007) 1193–1199. doi:10.1111/j.1551-
510 2916.2007.01532.x.
- 511 [13] Q. Li, Z. Sun, D. Tao, Y. Xu, P. Li, H. Cui, J. Zhai, Immobilization of simulated radionuclide
512 $^{133}\text{Cs}^+$ by fly ash-based geopolymer, *J. Hazard. Mater.* 262 (2013) 325–331.
513 doi:10.1016/j.jhazmat.2013.08.049.
- 514 [14] J.G. Jang, S.M. Park, H.K. Lee, Physical barrier effect of geopolymeric waste form on diffusivity
515 of cesium and strontium, *J. Hazard. Mater.* 318 (2016) 339–346.
516 doi:10.1016/j.jhazmat.2016.07.003.
- 517 [15] J. Wang, J.X. Wang, Q. Zhang, Y.X. Li, Immobilization of simulated low and intermediate level
518 waste in alkali-activated slag-fly ash-metakaolin hydroceramics, *Nucl. Eng. Des.* 300 (2016)
519 67–73. doi:10.1016/j.nucengdes.2016.01.011.
- 520 [16] Z. Li, T. Ohnuki, K. Ikeda, Development of Paper Sludge Ash-Based Geopolymer and
521 Application to Treatment of Hazardous Water Contaminated with Radioisotopes, *Materials*
522 (Basel). 9 (2016) 633. doi:10.3390/ma9080633.
- 523 [17] Z. Xu, Z. Jiang, D. Wu, X. Peng, Y. Xu, N. Li, Y. Qi, P. Li, Immobilization of strontium-loaded
524 zeolite A by metakaolin based-geopolymer, *Ceram. Int.* 43 (2017) 4434–4439.

- 525 doi:10.1016/j.ceramint.2016.12.092.
- 526 [18] J.L. Provis, P.A. Walls, J.S.J. van Deventer, Geopolymerisation kinetics. 3. Effects of Cs and Sr
527 salts, *Chem. Eng. Sci.* 63 (2008) 4480–4489. doi:10.1016/j.ces.2008.06.008.
- 528 [19] X. Peng, Y. Xu, Z. Xu, D. Wu, D. Li, Effect of Simulated Radionuclide Strontium on
529 Geopolymerization Process, *Procedia Environ. Sci.* 31 (2016) 325–329.
530 doi:10.1016/j.proenv.2016.02.043.
- 531 [20] K. Komnitsas, D. Zaharaki, G. Bartzas, Effect of sulphate and nitrate anions on heavy metal
532 immobilisation in ferronickel slag geopolymers, *Appl. Clay Sci.* 73 (2013) 103–109.
533 doi:10.1016/j.clay.2012.09.018.
- 534 [21] K. Gong, C.E. White, Impact of chemical variability of ground granulated blast-furnace slag on
535 the phase formation in alkali-activated slag pastes, *Cem. Concr. Res.* 89 (2016) 310–319.
536 doi:10.1016/j.cemconres.2016.09.003.
- 537 [22] J. Jang, S. Park, H. Lee, Cesium and Strontium Retentions Governed by Aluminosilicate Gel in
538 Alkali-Activated Cements, *Materials (Basel)*. 10 (2017). doi:10.3390/ma10040447.
- 539 [23] European Committee for Standardization, EN 196-6:2010 - Methods of testing cement - Part
540 6: Determination of fineness, 2010.
- 541 [24] N. Vandevenne, R.I. Iacobescu, Y. Pontikes, K. Gijbels, S. Schreurs, W. Schroevers, THE EFFECT
542 OF Cs AND Sr ON THE MECHANICAL PROPERTIES OF BLAST FURNACE SLAG INORGANIC
543 POLYMER FOR RADIOACTIVE WASTE IMMOBILISATION, in: 5th Int. Slag Valor. Symp., 2017:
544 pp. 401–404.
- 545 [25] ISO, International Standard ISO 10545-3:1995 - Determination of water absorption, apparent
546 porosity, apparent relative density and bulk density, 1997.
- 547 [26] ASTM, C 1220 - 98 Standard Test Method for Static Leaching of Monolithic Waste Forms for
548 Disposal of Radioactive Waste, (1998).
- 549 [27] European Committee for Standardization, CEN/TS 15863:2015: Characterisation of waste -
550 Leaching behaviour test for basic characterisation - Dynamic monolithic leaching test with
551 periodic leachant renewal, under fixed test conditions, 2015.
- 552 [28] E. Najafi Kani, A. Allahverdi, J.L. Provis, Calorimetric study of geopolymer binders based on
553 natural pozzolan, *J. Therm. Anal. Calorim.* (2016) 1–10. doi:10.1007/s10973-016-5850-7.
- 554 [29] J.G.S. van Jaarsveld, J.S.J. van Deventer, L. Lorenzen, Potential use of geopolymeric materials
555 to immobilize toxic metals: Part I. Theory and applications, *Miner. Eng.* 10 (1997) 659–669.
556 [http://dx.doi.org/10.1016/S0892-6875\(97\)00046-0](http://dx.doi.org/10.1016/S0892-6875(97)00046-0).
- 557